Contents list available at CBIORE journal website

International Journal of Renewable Energy Development

Journal homepage: https://ijred.cbiore.id

Review/Research Article

Experimental investigation of optimal blade pitch angle for a three-bladed H-Darrieus turbine under multi-directional tidal flow in Pantar Strait

Abdullah Apa[a]*, Haolia Rahman[b], Gun Gun Ramdlan Gunadi[b].

[a,b] Applied Master of Manufacturing Technology Engineering Postgraduate Study Program, Jakarta State Polytechnic, Jln. Prof. DR. G.A. Siwabessy, UI Indonesia Campus, Depok 16425

List of ORCID of each author
ORCID author 1: https://orcid.org/0009-0005-3440-7217
ORCID author 2: http://orcid.org/0000-0002-3414-7225
ORCID author 3: https://orcid.org/0000-0002-6010-9919

Abstract. Marine current energy has significant potential as a sustainable renewable energy resource due to its high energy density and predictable tidal characteristics. This study experimentally investigates the hydrodynamic and electromechanical performance of a small-scale Darrieus-H vertical-axis marine current turbine employing a symmetric NACA 0018 hydrofoil through in-situ field testing under real semidiurnal tidal flow conditions in the Pantar Strait, Indonesia. The turbine performance was evaluated at preset blade angles ranging from 5° to 30° to determine their influence on lift force, drag force, tangential force, torque, rotational speed, tip speed ratio (TSR), power coefficient, and electrical power generation. The turbine rotor had a diameter and height of 0.6 m and operated at an average current velocity of 1.60 m/s under a Reynolds number of approximately 1.06×10^6. The experimental results demonstrate that a fixed geometric blade angle of 15° yields the optimum performance, achieving a maximum power coefficient (Cp) of 0.262. At this operating condition, the turbine attained a rotational speed of 138.6 rpm, torque of 13.67 Nm, TSR of 2.72, mechanical power output of 198.3 W, and electrical power output of 144.1 W. Beyond 15°, turbine performance progressively deteriorated due to increasing flow separation and stall-related effects, resulting in higher drag and reduced rotational stability. The overall system efficiency reached 19.07%, while the generator maintained a relatively stable efficiency of 72.7%. The results indicate that the dominant energy losses occurred during the hydrodynamic energy extraction stage rather than during electromechanical conversion. These findings demonstrate the technical feasibility of small-scale marine current energy harvesting under real ocean operating conditions and highlight the importance of integrated optimization of rotor hydrodynamics, drivetrain configuration, and generator matching for improving overall system performance.

Keywords: Marine Current Power Plant, H-Darrieus Turbine, NACA 0018, Preset Blade Angle, Renewable Energy.

Received: xxx; Revised: xxxx; Accepted: xxx; Available online: xxx

1. Introduction

The increasing global energy demand, which is projected to continue growing over the coming decades, together with international commitments to reducing carbon emissions, has accelerated the development of renewable energy technologies in many countries (Fadllillah *et al.*, 2024; Ghafoorian *et al.*, 2025; Faisal *et al.*, 2026). In the context of tropical archipelagic countries and narrow strait regions such as Indonesia, the development of renewable energy has become highly important (Uchibori *et al.*, 2025), particularly to improve electricity accessibility in remote and outer island regions that are not yet fully connected to the national power grid (Presidential Regulation, 2023) A renewable energy contribution of 23% by 2025 and 31% by 2050 has been legally targeted under the Indonesian national energy roadmap to accelerate the transition away from fossil fuel dependency (Republic of Indonesia, 2014; Rifai *et al.*, 2021).

Among various marine renewable energy resources, hydrokinetic tidal current energy possesses highly promising potential and is considered one of the primary alternatives (Firmansyah, 2023; Boretti *et al.*, 2025) due to its energy density being approximately 835 times higher than that of air, as well as its relatively stable and predictable availability throughout the year (Madi *et al.*, 2025). Based on the national hydrokinetic energy mapping, Indonesia is estimated to possess a theoretical marine current energy potential of approximately ±17.9 GW concentrated within narrow strait corridors (Syahputra *et al.*, 2014; Madi *et al.*, 2022; Riansyah *et al.*, 2021). However, despite this substantial potential, its utilization as a basis for tidal current power generation development remains significantly underexploited.

One of the strategic locations with abundant hydrokinetic energy potential is the Pantar Strait in East Nusa Tenggara Province (NTT) (Prayoga *et al.*, 2019). This strait is characterized

by a semidiurnal tidal regime with current velocity fluctuations ranging from 0.6 to 3.5 m/(ESDM, 2020). The hydrodynamic behavior in this region is strongly influenced by irregular seabed bathymetry and strait constriction morphology, resulting in turbulent multi-directional flows, velocity shear, and circular current formations (eddy/vortex currents) (Havis *et al.*, 2014; Syahputra *et al.*, 2014). Such dynamic and complex marine environmental conditions indicate substantial power potential, estimated at approximately ±900 MW (Jatmiko *et al.*, 2025), while simultaneously presenting significant technical challenges regarding the mechanical durability and operational stability of energy conversion devices. Therefore, selecting turbine technology capable of adapting to multi-directional flow characteristics becomes a critical factor for successful energy extraction in this region.

To efficiently extract hydrokinetic energy, Vertical Axis Tidal Turbines (VATTs), particularly the H-Darrieus type, are considered more suitable than Horizontal Axis Water Turbines (HAWTs) (Cardenas *et al.*, 2025; Baihaqi *et al.*, 2025; Al-ghriybah, 2026; Gomez *et al.*, 2025). The primary advantage of the H-Darrieus turbine lies in its ability to capture fluid flow passively from multiple directions without requiring a complex and expensive yaw control system (Abhinaya *et al.*, 2026; Ghigo, 2024; Boulla *et al.*, 2025).

The use of standard symmetrical hydrofoils such as the NACA 0018 profile is preferred due to their good structural strength and ease of manufacturing (Mark Jason *et al.*, 2021). Nevertheless, the hydrodynamic performance of H-Darrieus turbines is highly sensitive to variations in geometric parameters and changes in preset blade angle (AOA) (Yunusa *et al.*, 2025; Abhinaya *et al.*, 2026). Improper AOA orientation may trigger premature flow separation on the blade surface, leading to dynamic stall phenomena. This phenomenon significantly reduces the turbine power coefficient (Cp). In addition, dynamic stall further deteriorates the self-starting capability of the turbine under low current velocity conditions (Shaaban *et al.*, 2025; Zhang *et al.*, 2026).

In response to these limitations, various aerodynamic and hydrodynamic blade optimization studies have been developed using modern Computational Fluid Dynamics (CFD) approaches (Michna *et al.*, 2024; Fertahi *et al.*, 2025). Numerous geometric innovations have been proposed to delay dynamic stall and improve turbine starting torque, including asymmetric J-shaped blade designs using micro-segment dimensional reduction approaches (Zhang *et al.*, 2026), blade profile and pitch angle modifications (Shaaban *et al.*, 2025), morphed airfoils obtained through sequential optimization methods (Zebedee *et al.*, 2024), as well as flow control technologies employing Dimple-Gurney Flaps (Jiang *et al.*, 2026) and bionic flexible flaps (Zhou, 2025).

In addition to external blade optimization, mechanical engineering improvements within the turbine transmission system have also been developed to maintain rotor rotational stability against torque ripple fluctuations. One widely adopted approach is the integration of dual flywheel systems functioning both as torque fluctuation dampers and transient kinetic energy storage devices to stabilize generator rotational speed (Marianus, 2019). In Indonesia, another approach involving Convergent Flow Disturbances (CoFD) has also been experimentally investigated to enhance turbine self-starting capability under low current velocity conditions (Madi *et al.*, 2025).

Although these studies have reported significant efficiency improvements, a considerable research gap still exists between theoretical findings and practical field implementation. Most blade optimization studies remain dominated by two-dimensional (2D) CFD simulations or laboratory-scale experiments under uniform linear flow conditions (Fertahi *et al.*, 2025; Yunusa *et al.*, 2025; Abhinaya *et al.*, 2026). In contrast, marine current conditions within Indonesian archipelagic waters are substantially more complex, being characterized by tidal fluctuations, circular vortices, and continuously changing flow directions.

Furthermore, most previous studies have tended to focus exclusively on blade hydrodynamics as an isolated aspect (Fawaz *et al.*, 2026; Chelabi, 2026). The influence of integrated system performance, including mechanical losses caused by bearing friction, gear transmission efficiency, rotating component inertia, and generator load compatibility with nonlinear hydrodynamic characteristics, has rarely been comprehensively investigated under real marine operating conditions.

To address these gaps, this study presents a direct in-situ experimental investigation on Preset Blade Angle optimization of a three-bladed H-Darrieus turbine based on the NACA 0018 profile operating under real circular current conditions in the Pantar Strait, East Nusa Tenggara. The main novelty of this research lies in its real-world in-situ testing approach, which integrates comprehensive performance analysis of the energy conversion system encompassing hydrodynamic, mechanical, and electrical aspects simultaneously.

Unlike previous studies that were predominantly based on idealized simulation approaches, this study evaluates the performance of a tidal current power generation prototype under complex multi-directional vortex current conditions to analyze the influence of Preset Blade Angle variation on self-starting time, shaft torque stability, and generator electrical power output efficiency simultaneously. The results of this study are expected to provide empirical data obtained directly from real marine environments while emphasizing the importance of integrated optimization between mechanical and electrical subsystems to improve the overall efficiency of tidal current power generation systems in tropical archipelagic strait regions.

2. Method

2.1 Blade chord design and geometry

The coordinates for the turbine installation were determined based on the specific hydrodynamic characteristics of the Pantar Strait, specifically at 8°17'24.06"S 124°18'21.07"E. This site is located within the narrow passage between Pura Island and the eastern tip of Pantar Island, spanning a distance of approximately 2-3 km. The selection of this location is strategic as the water mass flows semidiurnally with a multi-directional (circular) current pattern along this corridor.

This phenomenon is predominantly influenced by the complexity of the irregular seabed topography, the presence of small capes protruding into the sea along the passage, and the accumulation of large boulders on the strait floor, which collectively create controlled turbulence that supports circular flow patterns. The interaction between tidal currents and these topographical obstacles generates vortices and circular currents, which serve as the primary variables in evaluating the performance of the H-Darrieus turbine in this study.

2.2 Turbine design and specifications

The device employed in this study is a three-bladed H-Darrieus Vertical Axis Tidal Turbine (VATT). It utilizes the NACA 0018 symmetrical hydrofoil profile, selected for its

superior structural integrity and stable stall characteristics at high angles of attack (Rogelio *et al.*, 2025). The detailed specifications of the turbine and the design of the tidal current power plant are presented in Table 1 and Fig. 1, respectively.

Table 1. Technical specifications of the H-Darrieus tidal current turbine

MCTP Specifications	
Turbine Axis	Vertical
Darriues Turbine	Type H
Hydrofoil	NACA 0018
Number of blades	3 blades
Chord width	240 mm
Turbine dimensions H x D	600 x 600 mm
Radius of blade	300 mm
Propulsion method	Circular ocean currents
Geometric blade angle	5° - 30°
Seed depth	4 - 30 m
Tremona system	Anchor pontoon (semi-floating).
Generator rated power	500 W, 12-15 V,
Generator rated speed	500 RPM

Note: In this study, the blade pitch angle is fixed geometrically during each experimental run.

The turbine is integrated with a multi-stage mechanical transmission system, comprising a pair of bevel gears with a 1:1 ratio, a pulley-belt system with a 3:1 ratio, and an inertial flywheel stabilizer weighing approximately 15 kg to mitigate rotational fluctuations caused by current turbulence. This system is coupled to a Permanent Magnet Direct Current (PMDC) generator to convert mechanical energy into electrical power.

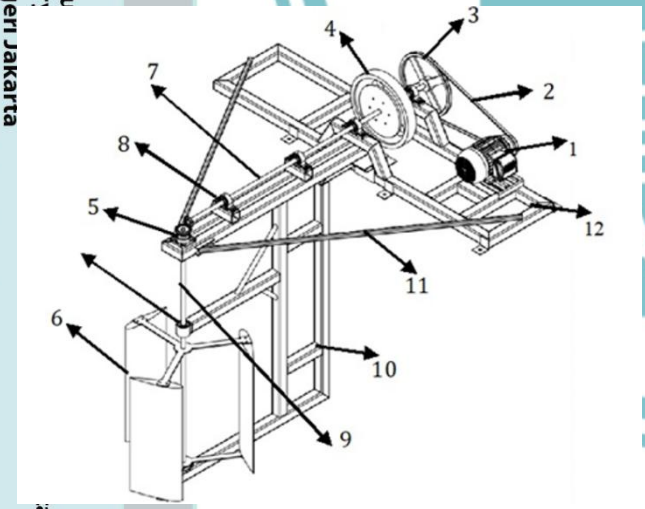

Fig. 1 Schematic design of the marine current turbine system.

The components of the marine current turbine prototype (MCTP) shown in Fig. 1 are described as follows :

1. DC generator
2. Fan
3. Pulley wheel
4. Flywheel
5. Bevel gear
6. Darrieus - H
7. Shaft (pulley wheel, flywheel and bevel gear)
8. Pillow block
9. Shaft (bevel gear and turbine)
10. Turbine mounting frame
11. Lap mounting frame
12. Lap frame

Fig. 2 (a) Installation of the MCPT on the pontoon, (b) The turbine in operation within the Pantar strait.

2.3 Experimental setup and procedures

The MCPT system was installed on a floating platform (pontoon) and secured using a mooring system to maintain stability during testing. The experiments were conducted at water depths ranging from 4 to 30 meters.

The tested geometric blade angle (α) were 5°, 10°, 15°, 20°, 25° and 30°. For each variation, the blade angle was adjusted accordingly and kept constant throughout the testing period.

All experiments were carried out under natural ocean current conditions. Data were collected at different times of the day (morning, afternoon, and night) to account for tidal variations. The turbine rotational speed (RPM) was measured under both no-load conditions and when coupled with a generator (loaded conditions).

The parameters measured in this study included ocean current velocity (m/s), turbine rotational speed (RPM), electrical voltage (V) and electric current (A).

The current velocity was measured using the float tracking (Lagrangian) method with multiple repetitions to improve accuracy. Voltage and current were measured using a voltmeter and ammeter, respectively, while turbine speed was recorded using a tachometer.

To ensure data reliability, the following procedures were applied: Each measurement was repeated several times. The reported data represent the average values of the measurements, data obtained under unstable (transient) conditions were excluded from the analysis.

The measurement location was approximately 3 km away from the center of the current (main flow), as the anchored mooring was not capable of withstanding the stronger forces at the core of the current flow.

In this study, the reported geometric blade angle refers to the preset geometric blade mounting angle relative to the local tangential direction of the turbine rotor. The blade setting angle was mechanically adjusted prior to each experimental run and maintained constant during turbine operation. Although the instantaneous effective Preset Blade Angle of a Darrieus turbine dynamically varies with azimuthal position and tip speed ratio, the present study focuses on the influence of fixed geometric blade angle configuration under real marine current conditions.

2.4 Ocean current data

The ocean current data used in this study were obtained from field measurements conducted in the Pantar Strait, Alor

Regency, East Nusa Tenggara, Indonesia. Ocean currents are generated by several physical mechanisms, including wind forcing, tidal interactions, density gradients, and gravitational effects, which collectively influence the movement of seawater masses (Mad *et al.*, 2025; Haqiqi, 2018). Narrow straits between islands typically exhibit higher current velocities due to tidal constriction effects, making them suitable locations for ocean current energy extraction.

The ocean current velocity data were obtained from measurements conducted by the center for marine technology research and development (Hatomi, 2011). This dataset represents current velocities measured at different water depths in the Pantar Strait and serves as a comparison with field observations. Current data at the site were collected using the Lagrangian method over approximately one month, covering peak high tide and low tide periods to capture the maximum and minimum current velocities, consistent with the site's semidiurnal tidal characteristics. Table 2 presents the minimum and maximum current velocities measured at depths ranging from 3 m to 27 m.

Table 2
Characteristics of ocean currents (Hatomi, 2011)

Depth (m)	Min. current velocity (m/s)	Max. current velocity (m/s)
3	0.011	3.436
5	0.004	3.676
7	0.011	3.531
9	0.016	3.462
11	0.015	3.441
13	0.014	3.505
15	0.026	3.527
17	0.014	3.350
19	0.014	3.283
21	0.006	3.087
23	0.010	3.105
25	0.019	2.928
27	0.015	2.381

Ocean currents contain kinetic energy that can be converted into mechanical energy using marine current turbines. The turbine blades capture the kinetic energy of the flowing water and convert it into rotational mechanical energy, which drives a generator to produce electrical power. (Balduzzi *et al.*, 2021; Khair *et al.*, 2021). This study uses measured ocean current velocity data as the primary input to determine turbine design parameters and to estimate turbine performance.

The kinetic power of ocean currents can be calculated using the following equation :

$$P = \frac{1}{2}\rho A V^3 \quad (1)$$

Where:
P = kinetic power of ocean currents (W)
ρ = density of sea water (kg/m³)
A = cross-sectional area of turbine (m²)
V = ocean current speed (m/s)

Where Cp is the dimensionless power coefficient, $P_{extracted}$ represents the mechanical power generated by the turbine rotor (W), ρ is the fluid density of the seawater (kg/m³), and A denotes the rotor swept area (m²). This metric serves as the primary indicator for the overall hydrodynamic efficiency of the symmetric NACA 0018 hydrofoil configuration.

2.5 Measurement uncertainty analysis

The experimental measurements were subjected to uncertainty analysis to evaluate the reliability and repeatability of the acquired data. The uncertainty estimation considered the accuracy specifications of all measuring instruments employed during the field experiment, including rotational speed, voltage, current, and flow velocity measurements. The instruments utilized in this study and their respective accuracies are summarized in Table 3

Table 3
Measurement Uncertainty

Parameter	Instrument	Accuracy
Rotational speed (RPM)	DT-2234C+ digital tachometer	± 0.05%
Voltage	Digital voltmeter	± 0.5%
Current	Clamp meter	± 1.5%
Flow velocity	Float tracking method	± 0.05 m/s

The uncertainty equation includes :

$$\frac{\Delta P}{P} = \sqrt{\left(\frac{\Delta V}{V}\right)^2 + \left(\frac{\Delta I}{I}\right)^2} \quad (2)$$

Where:
ΔP = *uncertainty of electrical power,*
ΔV = *voltage uncertainty,*
ΔI = *current uncertainty.*

An example of calculating measurement uncertainty analysis for electrical power is based on actual measurement data:
Voltage = 12.31 V
Current = 1.02 A
Total uncertainty = ± 1.37%

Using the measured electrical parameters of 12.31 V and 1.02 A, the propagated uncertainty of the electrical power measurement was calculated to be approximately ± 1.37%. This relatively low uncertainty indicates that the acquired electrical performance data are sufficiently reliable for engineering evaluation.

Each experimental condition was repeated three times under similar tidal conditions, and the average values were used for analysis to minimize random measurement fluctuations caused by ocean turbulence and wave disturbances. (Dharma *et al.*, 2018), as illustrated in Fig. 3

2.6 Turbine performance analysis

1. NACA 0018 hydrofoil

The hydrodynamic efficiency of the H-Darrieus turbine is significantly governed by the core geometric profile of the NACA 0018 hydrofoil. Rather than evaluating isolated profile parameters, this study focuses on how the collective foil geometry alters the lift-to-drag characteristics and pressure distribution under the dynamic tidal currents of the Pantar Strait (Dharma *et al.*, 2018), as illustrated in Fig. 3

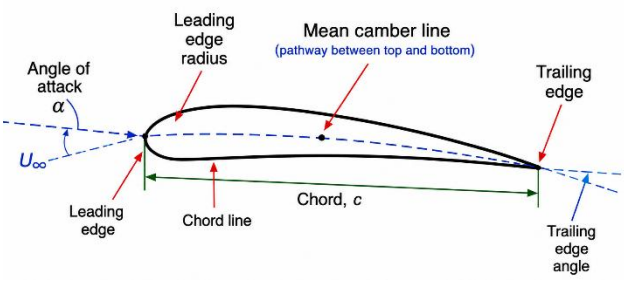

Fig. 3 Hydrofoil profile shape (Sudargana *et al.*, 2012)

The NACA hydrofoil profile is a simple aerodynamic geometry capable of generating lift force on a body through mathematical approaches used to predict the magnitude of the resulting lift force (Sahid et al., 2024; Şahin *et al.*, 2015; Abubakar *et al.*, 2015).

Prior numerical findings by (Loutun *et al.*, 2021) indicated that NACA 0018 outperformed other symmetric profiles with a peak power coefficient of 0.3. Conversely, a thinner profile like NACA 0010 yielded the minimum power coefficient but presented a broader operational range.

To make the NACA drawing process more precise, the chord length value must first be calculated using the following formula :

$$c = \frac{2\sigma\pi r}{B}(1 - \cos\theta) \quad (3)$$

Where : B = number of blades
σ = solidity (0.5)

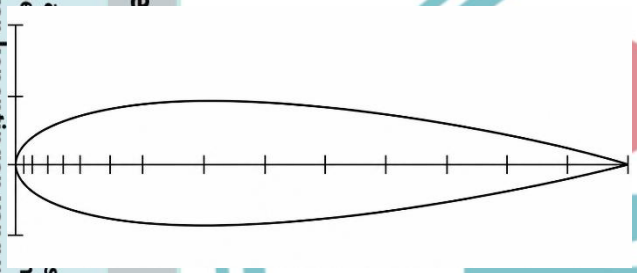

Fig. 4 NACA 0018 (Dharma et al., 2018; Nayeri et al., 2024)

2. Blade Geometry and Preset Blade Angle configuration

The geometric blade angle investigated in this study was varied systematically at 5°, 10°, 15°, 20°, 25°, and 30° by adjusting the preset blade mounting angle of the NACA 0018 hydrofoil relative to the turbine rotational path. These angle configurations were selected to represent the transition from low angle attached flow conditions to high angle stall dominant operating regimes.

At lower geometric angles (5°-10°), the hydrofoil generally operated under stable attached-flow conditions with relatively low drag generation, although the resulting lift force and torque production remained limited. Intermediate angles around 15° were expected to provide an optimum balance between lift enhancement and drag minimization, thereby improving turbine rotational performance and hydrodynamic energy extraction efficiency.

At higher geometric angles (20°-30°), the hydrofoil was expected to experience increasing flow separation, dynamic stall behavior, and wake instability, leading to deterioration of tangential force generation and reduced turbine performance. The selected angle range therefore allowed comprehensive evaluation of the influence of blade geometric configuration on the hydrodynamic and electromechanical characteristics of the Darrieus-H marine current turbine under real semidiurnal tidal flow conditions.

3. Torque *and power estimation*

The generated torque determines the mechanical power produced by the turbine shaft, which can then be transferred to a generator for electricity production. The torque is defined as :

$$T = \mathrm{F} \cdot \mathrm{r} \cdot \sin(\theta) \quad (4)$$

Where :
T = torque (N·m)
F = applied force (N)
r = rotor radius (m)
θ = angle between the force and the lever arm

According to Bernoulli's principle (Hatomi, 2011), the pressure difference between the upper and lower surfaces of the hydrofoil can be expressed as:

$$P_d + \frac{1}{2}\rho(v_r - v_c)^2 = P_z + \frac{1}{2}\rho(v_r + v_c)^2 \quad (5)$$

From this relation, the pressure difference is:
$\Delta P = P_d - P_z = 2\rho v_r v_c$
and the velocity difference becomes:
$\Delta v = \mathrm{v_c} - (-\mathrm{v_c}) = 2\mathrm{v_c}$
Thus, it can be written as:

$$P = \rho\, v_r\, \Delta v \quad (6)$$

Where :
ΔP = pressure difference between the upper and lower surfaces of the hydrofoil
Δv = velocity difference across the hydrofoil

The hydrodynamic forces acting on the turbine blades are influenced by fluid properties, flow velocity and blade geometry. The magnitude of this force can be calculated as :

$$F = \frac{1}{2}\rho v^2 c h C_L \quad (7)$$

Where :
F = hydrodynamic force (N)
ρ = seawater density (1025 kg/m³)
v = flow velocity (m/s)
c = blade chord length (m)
h = blade height (m)
C_L = lift coefficient

These relationships describe how fluid flow interaction with the hydrofoil generates lift forces, which in turn produce torque and drive the turbine rotation.

The mechanical energy generated by the Darrieus-H turbine is primarily produced by the tangential force resulting from hydrodynamic lift and drag interaction acting on the hydrofoil blades. To determine the power of the Darrieus turbine, the force and velocity vectors on the hydrofoil must first be known (Sudargana et al., 2012) Fig. 5. This is the force vector acting on the turbine, both lift and drag, as well as the tangential angle.

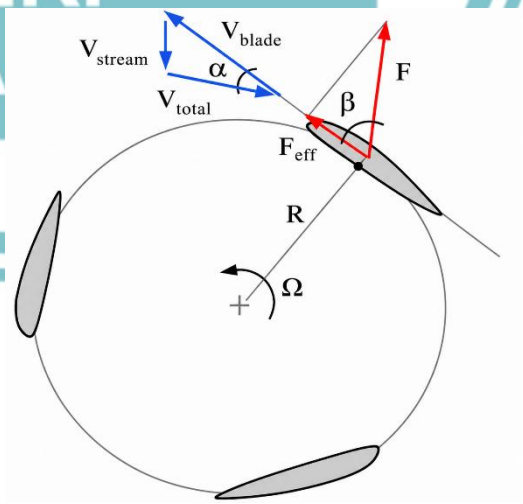

Fig. 5 Force on the turbine (Lopulalan, 2016, Chen *et al.*, 2023; Abbasi et al., 2024)

4. Tip speed ratio (TSR)

The tip speed ratio (TSR) is a key parameter used to evaluate turbine performance and is defined as :

$$TSR = \frac{u}{v} = \frac{\omega r}{v} \quad (8)$$

Where :

u = blade tip velocity (m/s)
v = flow velocity (m/s)
ω = angular velocity (rad/s)
r = turbine radius (m)

TSR represents the ratio between the blade rotational speed and the incoming flow velocity, and it significantly influences the efficiency of vertical axis turbines.

5. Force vectors and electrical power

The energy generated by a Darrieus turbine is shaft power derived from the kinetic energy of the water flow. To determine the power output of a Darrieus turbine, it is first necessary to analyze the force and velocity vectors acting on the hydrofoil (Sudargana *et al.*, 2012).Fig. 6 illustrates the force vectors acting on the turbine, including lift and drag forces along with their tangential angles, while Figure 7 shows the force and velocity vectors on the hydrofoil

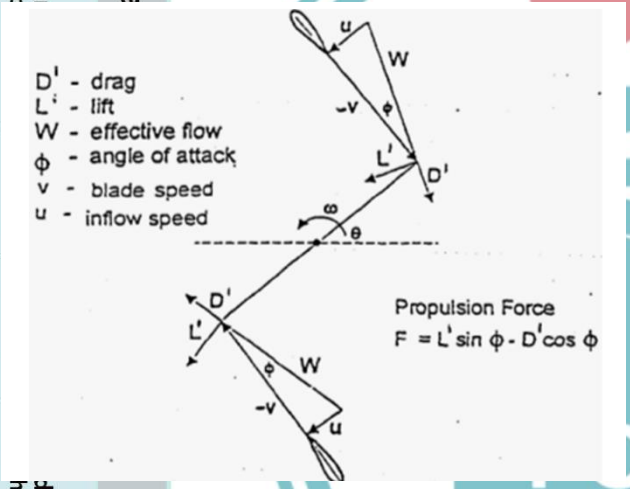

Fig. 6 Power coefficient and top speed ratio (TSR) graph (Rahman et al., 2016)

The equation of lift and drag on an airfoil or turbine blade is expressed as :

$$L = qAC_L \quad (9)$$

$$D = qAC_D \quad (10)$$

Where :

L = lift force (N)
D = drag force (N)
q = dynamic pressure of fluid(N/m^2)
C_L = lift coefficient
C_D = drag coefficient

The dynamic pressure equation is the fundamental equation used to calculate hydrodynamic forces acting on the blades of a Vertical Axis Marine Current Turbine (VAWT). The magnitude of each force can be expressed as follows :

$$F_L = \frac{1}{2}\rho V_{rel}^2 C_L A \quad (11)$$

$$F_D = \frac{1}{2}\rho V_{rel}^2 C_D A \quad (12)$$

ρ = fluid density (kg/m³) sea water ≈ 1025 kg/m³
V = fluid flow velocity (m/s)
A = reference area or cross-sectional area of the blade exposed to the flow (m²)

$$A = c \times h \quad (13)$$

Where:

c = airfoil chord
h = blade height.

Electrical power is the power produced by the rotation of the generator, the output power of the generator produced depends on the current and voltage.

$$P = V \times I \quad (14)$$

Where :

P = electrical power (Watts)
V = electric voltage (Volts)
I = electric current (Ampere)

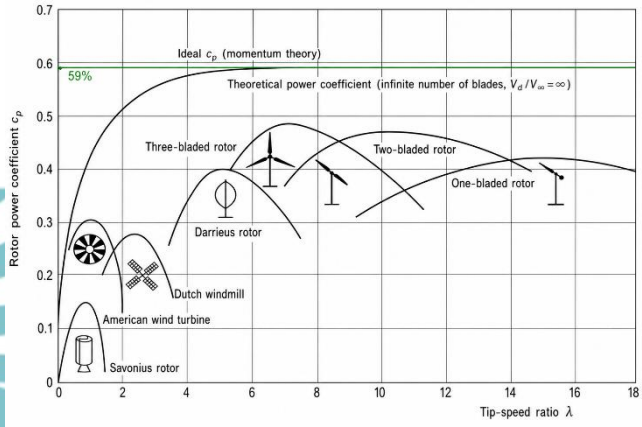

Fig. 7 Hydrofoil force and velocity vectors (Sudargana et al., 2012)

2.7 Hydrodynamic force estimation approach

The lift force, drag force, and tangential force presented in this study were not measured directly during the open-water experiments. Practical limitations associated with *in-situ* marine testing, particularly due to multidirectional semidiurnal tidal current conditions, rendered direct hydrodynamic force measurements using underwater load cells or multi-axis force transducers impractical.

Therefore, the hydrodynamic forces acting on the NACA 0018 hydrofoil were analytically estimated using classical hydrodynamic force equations based on the measured seawater current velocity and hydrofoil geometry. The lift and drag forces were calculated using the following equations:

$$F_L = \frac{1}{2}\rho V_{\text{rel}}^2 C_L A$$

$$F_D = \frac{1}{2}\rho V_{\text{rel}}^2 C_D A$$

Where :

- F_L= lift force (N)
- F_D= drag force (N)
- ρ= seawater density $(1025\ \text{kg/m}^3)$
- V_{rel}= relative flow velocity acting on the hydrofoil (m/s)
- C_L= lift coefficient
- C_D= drag coefficient
- A= projected blade area (m²), defined as: $A = c \times h$

where c is the chord length and h is the blade height (span). The lift and drag coefficients (C_L and C_D) for the NACA 0018 hydrofoil were obtained from previously published aerodynamic and hydrodynamic studies under comparable Reynolds number (Re) conditions within the order of 1.06×10^6. Furthermore, the tangential force contributing to rotor torque generation was estimated through vector decomposition of the lift and drag force components relative to the blade azimuthal position.

The calculated hydrodynamic force trends were then qualitatively validated by comparison with experimental performance parameters obtained from field testing in the Pantar Strait, including:

- turbine rotational speed,
- torque characteristics,
- tip speed ratio (TSR), and
- electrical power output.

The consistency observed between the analytical force trends and the actual turbine performance indicates that the hydrodynamic estimation approach adopted in this study provides a reasonable and sufficiently accurate representation of the turbine operational characteristics under real marine current conditions.

It should be noted that the calculated lift and drag forces represent simplified analytical estimations based on steady-state hydrodynamic assumptions and representative relative flow velocity conditions. Due to the inherently unsteady flow behavior of Darrieus-type turbines, including dynamic stall, azimuthal angle variation, wake interaction, and transient turbulence effects, the calculated force magnitudes should be interpreted primarily as comparative hydrodynamic indicators rather than exact instantaneous blade loading values.

2.3 Hydrodynamic force estimation approach

The lift coefficient (CL) and drag coefficient (CD) used in the present hydrodynamic force estimation were obtained from previously published NACA 0018 hydrofoil performance data under Reynolds number conditions comparable to the present study ($Re = 1.06 \times 10^6$). The selected coefficient values were adopted from experimental and numerical investigations reported in the literature for symmetric NACA-series hydrofoils operating under moderate-to-high Reynolds number marine flow conditions.

The adopted hydrodynamic coefficients for each geometric Preset Blade Angle were selected based on the pre-stall and post-stall behavior characteristics of the NACA 0018 profile. The coefficient trends were further evaluated qualitatively against the experimentally observed turbine rotational speed, torque behavior, and power output to ensure physical consistency between the analytical estimation and the field experiment results.

Table 4
Representative hydrodynamic coefficients adopted for analytical force estimation.

Geometric Blade angle, (°)	Lift coefficient, CL	Drag coefficient, CD
5	0.55	0.015
10	1.00	0.030
15	1.20	0.060
20	1.10	0.110
25	0.90	0.180
30	0.60	0.260

The representative lift and drag coefficients were adopted based on previously published aerodynamic and hydrodynamic performance characteristics of the symmetric NACA 0018 hydrofoil operating under moderate-to-high Reynolds number conditions. The selected coefficients reflect the typical pre-stall and post-stall behavior of NACA-series hydrofoils and were used for comparative analytical estimation of turbine hydrodynamic performance under different geometric blade angle configurations.

The adopted hydrodynamic coefficients were not intended to represent exact instantaneous blade operating conditions during turbine rotation, but rather to provide a simplified comparative hydrodynamic estimation framework under real marine current operating conditions.

3. Results and Discussion

3.1 Characteristics of ocean currents in the Pantar strait

The ocean current in the Pantar strait is characterized by semidiurnal tidal dynamics, where two flood tides and two ebb tides occur within a 24-hour period. Specifically, the current cycle at this location can be described as follows:

1. first flood tide phase (dawn-morning) : Water masses flow from the south (Sawu sea) toward the north (Flores sea). During this phase, the current velocity gradually increases and can reach a maximum value of approximately 2.75 m/s under normal astronomical conditions.
2. first ebb tide phase (afternoon) : A reversal of flow direction occurs, from the Flores sea toward the Sawu sea. The strait constriction effect results in relatively high current velocities during this phase, ranging from 1.5 to 3.5 m/s.
3. second flood tide phase (evening-night) : Water masses again flow northward, accompanied by a rising sea surface level.
4. second ebb tide phase (night-midnight) : The flow reverses once more toward the south, completing the daily semidiurnal cycle.

The variability of current velocity in the Pantar strait is strongly influenced by lunar cycles and moon phases. Under average conditions (neap and full moon transitions), the operational current velocity remains relatively stable. However, during spring tide conditions, current velocity can increase significantly to approximately 2.0-5.0 m/s due to stronger astronomical tidal forces. In contrast, during neap tide periods, the current energy decreases but generally remains above the turbine cut-in speed threshold.

The visualization of the daily semidiurnal current pattern is presented in Fig. 8, while the fluctuation between peak current phases and slack water conditions is illustrated in detail in Fig. 9. During slack water conditions, the turbine temporarily stops operating or rotates very slowly due to minimal flow velocity. The high velocity and repetitive flow pattern confirm the Pantar strait as a highly potential site for sustainable ocean current energy extraction.

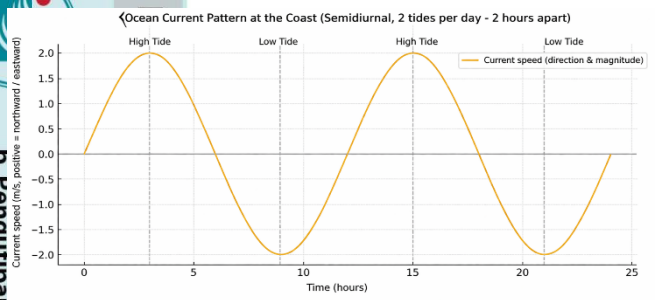

Fig. 8 Current pattern with 2 high tides and 2 low tides during 24 hours.

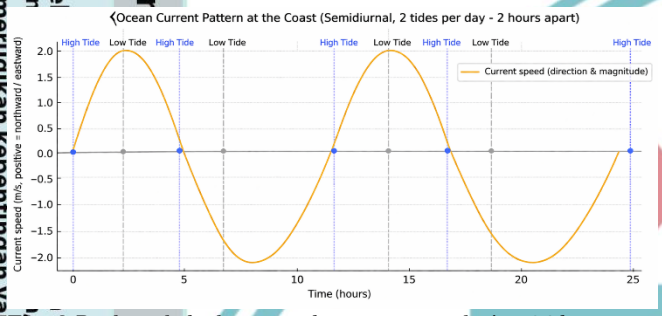

Fig. 9 Peak and slack water phase currents during 24 hours.

3.2 Determining the model and size of the chord

The turbine blade geometry in this study was designed using the symmetric NACA 0018 hydrofoil profile. The chord length (c) was determined analytically by considering the turbine solidity and rotor radius as the primary design parameters. The airfoil coordinates were generated using the standard NACA thickness distribution equations to obtain an accurate and mathematically consistent geometric representation.

The calculation results presented in Table 5 show that the maximum thickness of the profile, equal to 18% of the chord length, is located at approximately 30% of the chord from the leading edge, which is consistent with the characteristics of the NACA 0018 profile. The coordinate plot shown in Fig. 10 illustrates a smooth and continuous surface curve without geometric discontinuities. The profile was subsequently extruded into a three-dimensional model for further hydrodynamic analysis.

To make the NACA 0018 drawing process more precise, the chord length value must be calculated first, which is obtained from the equation below and the calculation results (x) and (-y_t) are obtained as in Table 5 :

$\bar{c} = \frac{c}{D}$, so the actual chord length is $c = \bar{c} \cdot D$.

$c = \frac{2\sigma\pi r}{B}(1 - \cos\theta)$

Where is the variable of :

$\pm$ yt (x) = c$\cdot \frac{t}{0.2}$ (0.2969$\frac{x}{c}$ − 0.1260$\frac{x}{c}$ − 0.3516 $(\frac{x}{c})^2$ + 0.2843$(\frac{x}{c})^3$−0.1015$(\frac{x}{c})^4$

Table 5
NACA 0018 calculation from x to -y_t

x (m)	x/c	+ y_t (m)	− y_t (m)
0.00	0.00	0.0000	0.0000
0.04	0.167	0.0416	- 0.0416
0.08	0.333	0.0521	- 0.0521
0.12	0.500	0.0532	- 0.0532
0.16	0.667	0.0476	- 0.0476
0.20	0.833	0.0378	- 0.0378
0.24	1.000	0.0000	0.0000

From the data in Table 5 NACA 0018 can be described as can be seen in Fig. 10 and then used to make blades on turbines.

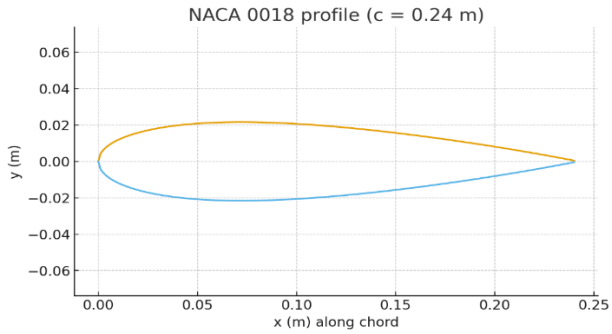

Fig. 10 NACA 0018 calculation

3.3 Reynolds number characterization

The hydrodynamic performance of the NACA 0018 hydrofoil was characterized using Reynolds number analysis to determine the flow regime experienced by the turbine during field operation in the Pantar Strait. Reynolds number is a critical parameter governing boundary layer behavior, flow separation characteristics, and lift to drag performance of hydrofoil based vertical axis turbines.

The Reynolds number was calculated using :

$$Re = \frac{\rho V_{rel} c}{\mu}$$

Where :

$\rho = 1025$ kg/m³
$V_{rel} = 4.64\ m/s$
$c = 0.24$ m
$\mu = 0.00108$ Pa.s

Yields :

$$Re = \frac{(1025)(4.64)(0.24)}{0.00108}$$
$$Re = 1{,}056{,}852$$
$$Re = 1.06 \times 10^6$$

The obtained Reynolds number indicates that the turbine operates within a medium-to-high Reynolds number regime, where turbulent boundary layer effects become dominant. Under these conditions, the hydrodynamic performance of the NACA 0018 hydrofoil is significantly influenced by turbulent flow behavior, particularly in terms of lift generation, drag characteristics, and stall development. The relatively high Reynolds number also suggests improved flow attachment over the hydrofoil surface before the onset of flow separation at higher angles of attack.

This Reynolds number range is consistent with the observed increase in lift force up to an Preset Blade Angle of 15°, where the hydrofoil still operates predominantly within the pre-stall regime.

3.4 Effect of AoA on hydrodynamic and tangential forces

Fig. 11 Illustrates the relationship between the AoA and the lift force generated by the NACA 0018 hydrofoil. The lift force increases significantly as the AoA rises from 5° to 15°. At 5°, the lift force is 874.1 N and increases to 1589.3 N at 10°, before reaching a maximum value of 1907.2 N at 15°. This phenomenon indicates that the hydrofoil operates predominantly within the pre-stall regime, where the increase in Preset Blade Angle enhances the pressure difference between the upper and lower surfaces of the hydrofoil, thereby increasing lift generation.

Beyond 15°, the lift force decreases sharply. At 20°, the lift drops to 1782.2 N and further decreases significantly to 953.6 N at 30°. This reduction indicates the onset and progression of flow separation over the hydrofoil surface, leading to stall conditions. Under stall conditions, the separated flow reduces the effective circulation and pressure difference around the hydrofoil, thereby significantly decreasing the lift-producing capability of the hydrofoil.

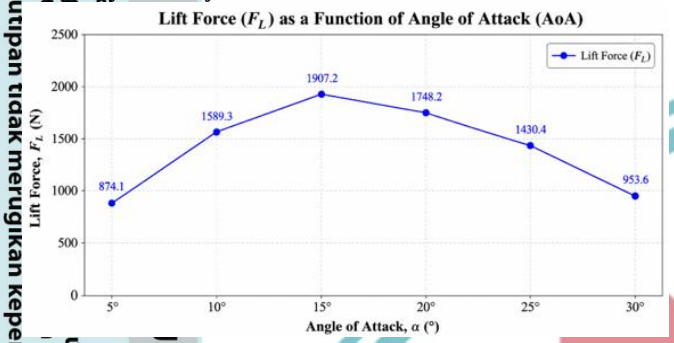

Fig. 11 The lift force versus AoA

Fig. 12 presents the variation of drag force (F_D) with the angle of attack (AoA) for the NACA 0018 hydrofoil. The drag force increases continuously from 23.8 N at 5° to 413.2 N at 30°, indicating a progressively stronger resistance to the incoming flow. At low AoA (5°-15°), the increase in drag remains moderate, suggesting that the flow is largely attached to the hydrofoil surface. However, beyond 15°, the drag force rises rapidly, reaching 174.8 N at 20°, 286.1 N at 25°, and 413.2 N at 30°. This behavior is attributed to the development of adverse pressure gradients and flow separation, which increase pressure drag and hydrodynamic losses.

The sharp drag escalation at higher AoA indicates the onset and progression of stall, where a significant portion of the available flow energy is dissipated rather than converted into useful torque. When considered together with the lift-force and power-coefficient results, the findings indicate that an AoA of 15° provides the most favorable lift-to-drag ratio and represents the optimum operating condition for maximizing the hydrodynamic performance of the proposed Darrieus-H marine current turbine..

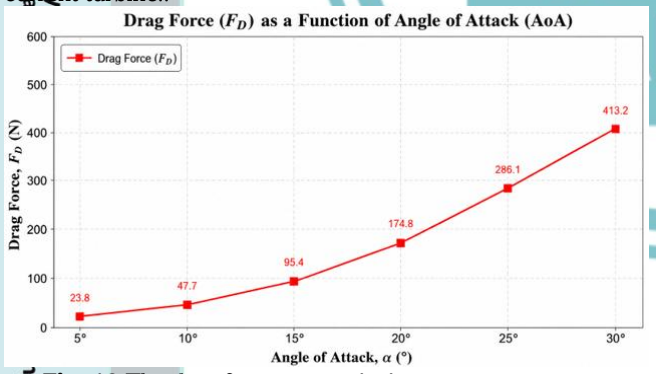

Fig. 12 The drag force versus AoA

Fig. 13 illustrates the variation of instantaneous tangential force ($F_{t,inst}$) and average tangential force ($F_{t,avg}$) with the angle of attack (AoA). Both parameters increase with AoA from 5° to 15°, reaching maximum values of 569.5 N and 45.6 N, respectively. This trend indicates enhanced lift generation under pre-stall conditions, where the flow remains attached to the hydrofoil surface and produces an effective tangential force component.

Beyond 15°, both $F_{t,inst}$ and $F_{t,avg}$ decrease significantly and become negative at 30°. This behavior is associated with flow separation and stall development, which reduce lift while increasing drag. Consequently, the effective tangential force available for torque production decreases, and the negative values at 30° indicate an adverse torque contribution caused by drag dominance.

The results confirm that an AoA of 15° provides the optimum hydrodynamic operating condition within the investigated range. The maximum tangential force obtained at this angle is consistent with the highest lift-to-drag ratio, thereby maximizing rotor torque and enhancing the overall performance of the proposed Darrieus-H marine current turbine.

Fig. 13 The tangential force versus AoA.

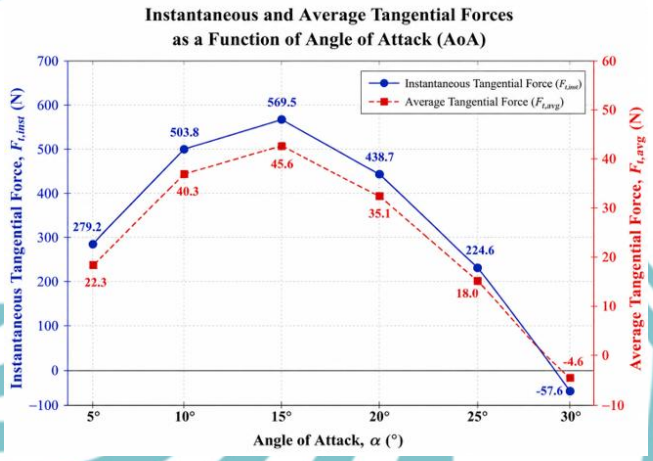

3.5 Analysis of Torque, Turbine Rotational Speed, and Power Coefficient (Cp)

Fig. 14 presents the variation of average torque with the angle of attack (AoA). The torque increases from 6.70 Nm at 5° to a maximum value of 13.67 Nm at 15°, indicating improved hydrodynamic loading and more effective conversion of lift force into rotational motion. Within this range, the increase in AoA enhances the pressure difference across the hydrofoil surface, resulting in higher lift generation and consequently greater tangential force and rotor torque.

Beyond 15°, the torque decreases progressively to 10.53 Nm at 20° and 5.39 Nm at 25°, before becoming negative (-1.38 Nm) at 30°. This decline is primarily attributed to flow separation and stall development, which reduce lift while increasing drag. As a result, the effective tangential force available for torque generation decreases significantly. The negative torque observed at 30° indicates that drag forces dominate the hydrodynamic response, producing an adverse effect on rotor rotation.

The torque distribution confirms that an AoA of 15° provides the optimum operating condition within the investigated range. This finding is consistent with the maximum lift force, tangential force, and power coefficient obtained at the same AoA. Since mechanical power is directly proportional to torque ($P = T\omega$), the peak torque at 15° corresponds to the highest power extraction capability, making this angle the most favorable configuration for maximizing the performance of the proposed Darrieus-H marine current turbine.

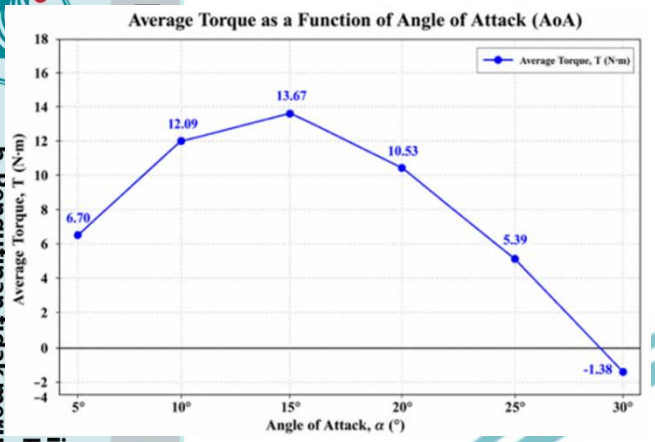

Fig. 14 Graph of total torque vs AoA

Fig. 15 shows the variation of turbine rotational speed with the angle of attack (AoA). The rotational speed increases from 88.5 rpm at 5° to a maximum value of 138.6 rpm at 15°, representing enhanced lift generation and torque production under pre-stall conditions. Beyond 15°, the rotational speed decreases progressively, reaching 74.9 rpm at 30° due to flow separation and increasing drag. The trend is consistent with the torque and power-coefficient results, confirming that an AoA of 15° provides the optimum hydrodynamic operating condition for maximizing turbine performance.

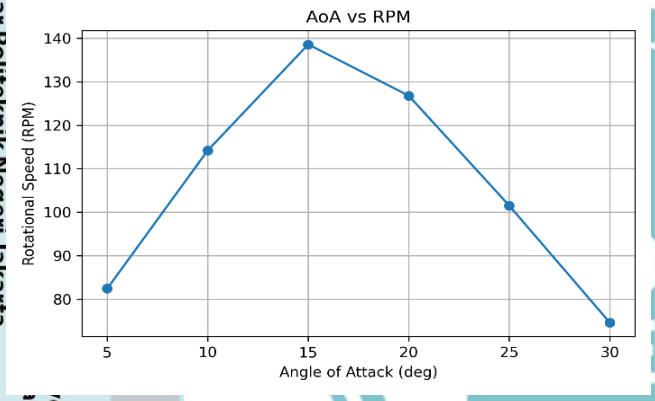

Fig. 15 Relationship between AoA and turbine rotational speed

Fig. 16 shows the variation of tip speed ratio (TSR) with the angle of attack (AoA). The TSR increases from 1.62 at 5° to a maximum value of 2.72 at 15°, reflecting enhanced hydrodynamic performance and more efficient energy extraction. Beyond 15°, the TSR decreases progressively due to flow separation and stall effects, reaching 1.46 at 30°. This trend is consistent with the torque, rotational speed, and power-coefficient results, confirming that an AoA of 15° provides the optimum operating condition for the proposed Darrieus-H marine current turbine.

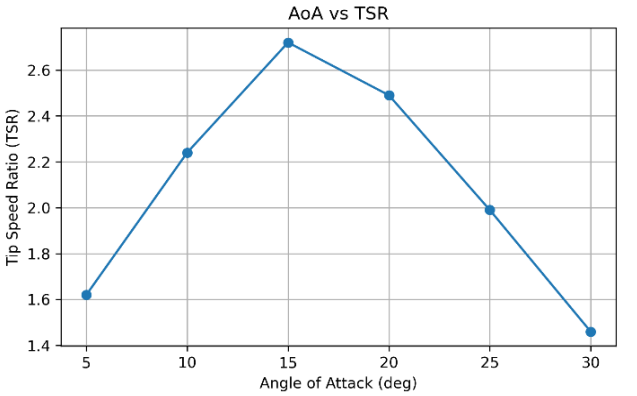

Fig. 16 Relationship between AoA and tip speed ratio

Fig. 17 presents the variation of power coefficient (C_p) with the angle of attack (AoA). The C_p increases from 0.129 at 5° to a maximum value of 0.262 at 15°, indicating the most efficient energy extraction condition. Beyond 15°, the C_p decreases progressively and becomes negative at 30° due to the increasing influence of flow separation and stall. This trend is consistent with the corresponding reductions in tangential force, torque, rotational speed, and TSR, confirming that an AoA of 15° provides the optimum operating condition for maximizing the performance of the proposed Darrieus-H marine current turbine.

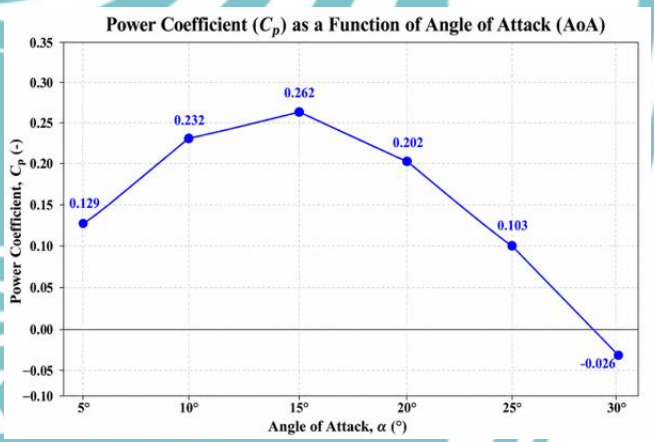

Fig. 17 Relationship between AoA and power coefficient

Fig. 18 presents the variation of mechanical power, generator power, and generator efficiency with the angle of attack (AoA). Both mechanical and generator power increase with AoA from 5° to 15°, reaching maximum values of 198.3 W and 144.1 W, respectively. This trend is consistent with the corresponding increases in lift force, tangential force, torque, rotational speed, and power coefficient, indicating more effective energy extraction under pre-stall conditions.

Beyond 15°, both power outputs decrease significantly, falling to 117.8 W and 85.6 W at 20°, and further to 30.9 W and 22.5 W at 25°. At 30°, the power output approaches zero, reflecting the severe degradation of turbine performance due to stall-induced hydrodynamic losses. The reduction in power is primarily associated with flow separation, which decreases lift generation while increasing drag, thereby reducing the torque available for power production.

The generator efficiency remains constant at 72.67% throughout the investigated operating range, indicating stable

generator performance. Therefore, variations in electrical power output are mainly governed by the turbine hydrodynamic characteristics rather than generator efficiency. The maximum mechanical and electrical power obtained at 15° confirms that this AoA provides the optimum operating condition for the proposed Darrieus-H marine current turbine.

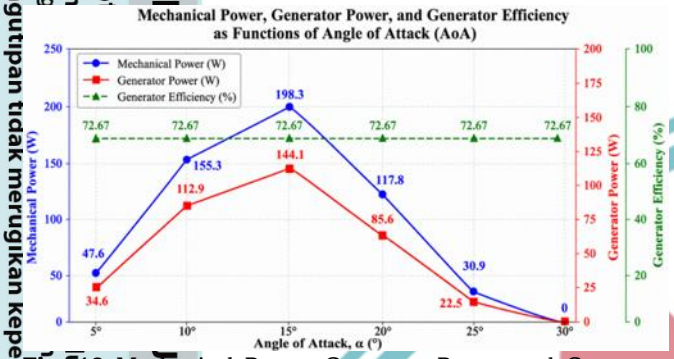

Fig. 18 Mechanical Power, Generator Power, and Generator Efficiency

Fig. 19 shows the relationship between the available marine current power, generator power, and overall system efficiency as a function of AoA. The available marine current power remains constant at 755.7 W for all operating conditions because the flow velocity and turbine swept area are unchanged. In contrast, the generator power varies significantly with AoA, reaching a maximum value of 144.1 W at 15°.

As a consequence, the overall system efficiency increases from 4.58% at 5° to a peak value of 19.07% at 15°, before decreasing to 11.33% at 20° and 2.98% at 25°. At 30°, the system efficiency drops to zero due to the inability of the turbine to produce useful power under severe stall conditions. The efficiency trend closely follows the variations in torque, rotational speed, and power coefficient, highlighting the strong dependence of system performance on hydrodynamic behavior. The highest system efficiency achieved at 15° confirms that this AoA provides the most effective conversion of marine current energy into electrical power. This finding is consistent with the maximum values of lift force, tangential force, torque, TSR, rotational speed, power coefficient, and generator output obtained at the same operating condition, thereby establishing 15° as the optimum design angle for the proposed Darrieus-H marine current turbine.

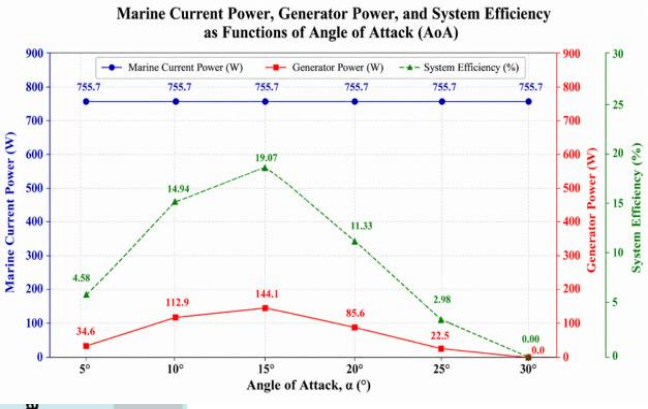

Fig. 19 Marine Current Power, Generator Power, and System Efficiency

3.6 *Evaluation of power and system efficiency*

The performance of the proposed marine current turbine was evaluated by analyzing the conversion of available hydrodynamic power into useful electrical output power. The available marine current power was calculated using:

$$P_a = \frac{1}{2}\rho A V^3$$

where $\rho$is the seawater density, $A$is the turbine swept area, and $V$is the incoming current velocity. For the present turbine configuration, the swept area was determined as:

$$A = D \times H$$
$$A = 0.6 \times 0.6 = 0.36\ m^2$$

Using a seawater density of 1025 kg/m³ and an average current velocity of 1.60 m/s, the available marine current power was calculated to be 755.7 W.

The maximum mechanical power generated by the turbine was obtained at an AoA of 15°, reaching 198.3 W. The corresponding power coefficient was calculated as:

$$C_p = \frac{P_m}{P_a}$$
$$C_p = \frac{198.3}{755.7} = 0.262$$

This result indicates that approximately 26.2% of the available kinetic energy in the marine current was converted into useful mechanical power. The obtained $C_p$is consistent with the optimum hydrodynamic condition identified from the lift force, tangential force, torque, rotational speed, and TSR analyses.

The electrical power delivered by the generator reached a maximum value of 144.1 W at the same operating condition. Accordingly, the generator efficiency was calculated as:

$$\eta_g = \frac{P_g}{P_m} \times 100$$
$$\eta_g = \frac{144.1}{198.3} \times 100 = 72.67\%$$

The relatively constant generator efficiency observed throughout the investigated operating range indicates stable electromechanical energy conversion performance.

The overall system efficiency, defined as the ratio between electrical output power and available marine current power, was determined as:

$$\eta_{sys} = \frac{P_g}{P_a} \times 100$$
$$\eta_{sys} = \frac{144.1}{755.7} \times 100 = 19.07\%$$

Although the generator efficiency remained relatively high, the overall system efficiency was limited to 19.07% due to hydrodynamic losses associated with flow separation, wake formation, and mechanical transmission losses within the turbine drivetrain. These losses reduced the amount of available marine current energy that could be converted into useful electrical power.

The maximum system efficiency obtained at an AoA of 15° is consistent with the peak values of power coefficient, torque, rotational speed, and generator power. Therefore, an AoA of 15° is identified as the optimum operating condition for maximizing the overall performance of the proposed Darrieus-H marine current turbine under semidiurnal tidal current conditions

Table 6
Energy conversion performance of the proposed turbine system

Parameter	Value
Available marine current power (W)	755.7
Mechanical turbine output power (W)	198.3

Electrical output power (W)	144.1
Power coefficient, C_p(%)	26.2
Generator efficiency, η_g(%)	72.7
Overall system efficiency, η_{sys}(%)	19.07

3.7 Energy loss analysis

To evaluate the effectiveness of the energy conversion process, an energy loss analysis was conducted across the hydrodynamic, mechanical, and electrical conversion stages. The available marine current power under the measured flow conditions was calculated as 755.7 W. At the optimum angle of attack (AoA) of 15°, the turbine produced a maximum mechanical power output of 198.3 W, corresponding to a power coefficient (C_p) of 0.262.

The mechanical power was subsequently transmitted to the generator through the drivetrain system, resulting in an electrical output power of 144.1 W. Based on these values, the generator efficiency was determined to be 72.67%, while the overall system efficiency relative to the available marine current power reached 19.07%.

The energy conversion process reveals that approximately 73.8% of the available marine current energy was not converted into useful mechanical power due to hydrodynamic losses associated with wake formation, flow separation, tip losses, and other rotor-flow interaction effects. Furthermore, additional losses occurred during the electromechanical conversion stage, where approximately 27.3% of the mechanical power was not converted into electrical power.

These results indicate that the dominant energy losses originated from the hydrodynamic conversion stage rather than the generator system. Although the generator exhibited a relatively stable efficiency of 72.67%, only a fraction of the available marine current energy was captured by the turbine rotor. Therefore, future performance improvements should primarily focus on enhancing rotor hydrodynamics through blade optimization, improved operating TSR, and reduction of flow separation effects. Additional gains may also be achieved through drivetrain refinement and generator matching to the turbine operating characteristics.

3.8 Integrated performance discussion

The overall performance evaluation demonstrates that the hydrodynamic behavior of the turbine strongly influences the subsequent mechanical and electrical energy conversion processes. Among the investigated operating conditions, an angle of attack (AoA) of 15° consistently produced the highest lift force, tangential force, torque, rotational speed, tip speed ratio (TSR), power coefficient, mechanical power, electrical power, and system efficiency. This confirms that the turbine operated under its optimum hydrodynamic condition at this AoA.

At the optimum operating point, the turbine generated a maximum mechanical power of 198.3 W from an available marine current power of 755.7 W, corresponding to a power coefficient ((C_p)) of 0.262. The electrical output power reached 144.1 W, resulting in a generator efficiency of 72.67% and an overall system efficiency of 19.07%. These results indicate that the generator exhibited relatively stable electromechanical conversion performance, while the major energy losses originated from the hydrodynamic conversion stage.

The reduction in performance observed beyond 15° is primarily associated with the onset and progression of flow separation and stall. As the angle of attack increased, lift generation decreased while drag increased, leading to reductions in tangential force, rotor torque, rotational speed, TSR, and power coefficient. Consequently, both mechanical and electrical power outputs declined significantly at higher AoA values. At 30°, severe stall conditions resulted in negligible power generation and zero system efficiency.

The results highlight the importance of integrated optimization in marine current energy conversion systems. Although the turbine demonstrated satisfactory hydrodynamic performance under real semidiurnal tidal current conditions, further improvements may be achieved through enhanced blade design, reduction of drivetrain losses, and improved matching between turbine operating characteristics and generator requirements. Such developments are expected to increase overall energy conversion efficiency and improve the practical viability of small-scale marine current turbines for renewable energy applications.

3.9 Validation with previous studies

To assess the reliability of the experimental results, the performance of the proposed Darrieus-H marine current turbine was compared with several previous numerical and experimental studies involving NACA-series hydrofoils and H-Darrieus turbines. Table 7 summarizes the reported power coefficient (*Cp*) ranges from the literature and compares them with the maximum value obtained in the present study.

.

Table 7
Validation with Previous Studies

Study	Turbine/Method	Reported Cp Range
Loutun et al. (2021)	CFD Simulation	0.24-0.38
Boulla et al. (2025)	CFD Simulation	0.26-0.41
Rogelio et al. (2025)	Experimental Study	0.18-0.32
Gomez et al. (2025)	Numerical Hydrokinetic Study	0.20-0.36
Present study	Field Experiment	0.26

The maximum power coefficient achieved in this study (Cp = 0.262) falls within the ranges reported by previous investigations, including Loutun et al. (2021) (0.24-0.38), Boulla et al. (2025) (0.26-0.41), Rogelio et al. (2025) (0.18-0.32), and Gomez et al. (2025) (0.20-0.36). This agreement indicates that the hydrodynamic performance of the proposed turbine is consistent with established H-Darrieus turbine characteristics reported in the literature.

Although the obtained (Cp) is lower than the upper limits reported in several CFD-based studies, such differences are expected because the present investigation was conducted under real marine current conditions in the Pantar Strait. Unlike idealized numerical simulations, field conditions involve turbulence, multidirectional flow effects, velocity fluctuations, and temporal variations in current direction, all of which influence turbine performance and energy extraction efficiency.

Overall, the close agreement between the present experimental results and previous studies validates the hydrodynamic behavior of the proposed turbine and demonstrates the practical applicability of the Darrieus-H concept for small-scale marine current energy conversion under realistic operating conditions.

3.10 Study limitations

The present study has several limitations that should be considered when interpreting the results. First, the hydrodynamic lift and drag forces were estimated using analytical approaches based on representative hydrodynamic

coefficients rather than direct underwater force measurements. Consequently, the reported force values should be interpreted as performance indicators for comparative analysis rather than exact blade loading conditions.

Second, the experimental investigation was conducted under real semidiurnal tidal current conditions over a limited observation period. Therefore, long-term effects such as seasonal current variability, structural degradation, and biofouling were not evaluated. In addition, the open-water environment introduced unavoidable fluctuations in flow velocity, turbulence intensity, and flow direction, which may have affected turbine performance and measurement repeatability.

Furthermore, detailed CFD validation, transient fluid–structure interaction analysis, and direct measurement of the instantaneous blade angle of attack were beyond the scope of this study. As a result, the investigation focused primarily on evaluating the influence of preset blade angle on turbine performance under realistic operating conditions.

Future work should incorporate CFD-based validation, direct hydrodynamic force measurements, uncertainty quantification, advanced flow visualization techniques, and long-term field deployment. These improvements are expected to provide a more comprehensive understanding of turbine hydrodynamics and support the development of more efficient marine current energy conversion system.

4. Conclusion

This study experimentally investigated the performance of a NACA 0018-based Darrieus-H marine current turbine under actual semidiurnal tidal current conditions in the Pantar Strait, Indonesia. The results demonstrate the feasibility of utilizing local marine current resources for small-scale renewable energy generation and provide valuable field-scale performance data under realistic operating conditions.

Among the investigated operating configurations, an angle of attack (AoA) of 15° yielded the optimum turbine performance. At this condition, the turbine achieved the highest lift force, tangential force, torque, rotational speed, tip speed ratio (TSR), power coefficient, mechanical power, and electrical power output. The maximum mechanical power generated by the turbine reached 198.3 W from an available marine current power of 755.7 W, corresponding to a power coefficient (Cp) of 0.262. The electrical output power reached 144.1 W, resulting in a generator efficiency of 72.67% and an overall system efficiency of 19.07%.

The performance degradation observed beyond 15° was primarily attributed to flow separation and stall development, which reduced lift generation and increased drag. Consequently, the tangential force, rotor torque, rotational speed, TSR, power coefficient, and power output decreased significantly at higher angles of attack. These findings confirm that hydrodynamic optimization plays a critical role in maximizing marine current energy extraction.

Comparison with previous numerical and experimental studies showed that the obtained power coefficient falls within the range reported in the literature, validating the hydrodynamic performance of the proposed turbine configuration. More importantly, this study provides experimental evidence obtained under real marine current conditions, where turbulence, multidirectional flow effects, and temporal flow fluctuations continuously influence turbine operation.

Overall, the results demonstrate that a preset blade angle of 15° represents the optimum operating condition for the proposed Darrieus-H marine current turbine. The findings contribute to the development of practical marine current energy conversion systems and provide a foundation for future improvements involving blade optimization, drivetrain refinement, generator matching, and advanced power management strategies to further enhance overall system efficiency.

Acknowledgments
The author would like to thank the Jakarta State Polytechnic community, Mr. Haolia Rahman, Mr. Gun Gun Ramdlan Gunadi as academic supervisor, as well as Saban Rasid and his family for their valuable assistance during the field research process and all other parties who have provided support in the design and research process.

Author Contributions: **Abdullah Apa** : Conceptualization, methodology, formal analysis, writing-original draft, **Haolia Rahman** ; supervision, resources, project administration, **Gun Gun Ramdlan Gunadi** ; writing-review and editing, project administration, validation. All authors have read and agreed to the published version of the manuscript.

Funding: This research was funded or received assistance from the Jakarta State Polytechnic through the Final Year Student Research (PMTA) program..

Conflicts of Interest: The authors declare no conflict of interest.

References

Abbasi, S. & Daraee, M.A. (2024) 'Ameliorating a vertical axis wind turbine performance utilizing a time - varying force plasma actuator', Scientific Reports, pp. 1-18. Available at: https://doi.org/10.1038/s41598-024-69455-8.

Abhinaya, V., & Kumar, G. G. (2026). A comprehensive review on H-type Darrieus wind turbine: Aerodynamics, blade profile, CFD simulations. *Journal of engineering and applied science*, 73(1), Article 106. https://doi.org/10.1186/s44147-026-00968-x.

Abubakar, M. A., Bawa, M. A., Muhammad, M. H., & Dandakouta, H. (2025). Design, optimization, and determination of lift and drag forces of NACA aerofoils for enhanced performance. *Unizik journal of technology, Production and mechanical systems (UJTPMS)*, *6*(1), 285–296. https://journals.unizik.edu.ng/index.php/ujtpms/article/view/5993.

Al-ghriybah, M. (2026) 'Vertical-Axis Wind turbines for extreme environments : a systematic review of performance , Adaptation Challenges, and future pathways'. https://doi.org/10.3390/inventions11020025.

Baihaqi, R. *et al.* (2025) "The effect of blade angle variations on the Darrieus type H vertical wind turbine on wind turbine performance", *Jurnal Flywheel*, *16*(1), pp. 1–6. Available at: https://doi.org/10.36040/flywheel.v16i1.9483.

Balduzzi, F. *et al.* (2021) 'Some design guidelines to adapt a Darrieus vertical axis turbine for use in hydrokinetic applications', 08017, pp. 1–12. https://doi.org/10.1051/e3sconf/202131208017.

Boretti, A. & Castelletto, S. (2025) 'Advancements and challenges in tidal stream and oceanic current turbines: an overview of current technologies and future prospects', *Marine development*, *3*(1). Available at:

https://doi.org/10.1007/s44312-025-00054-5.

Boulla, D. *et al.* (2025) 'Enhancement of aerodynamic performance of H-Darrieus rotor using wraparound fairing system: A 2D CFD study', *International journal of renewable energy development*, *14*(5), pp. 1058–1071. Available at: https://doi.org/10.61435/ijred.2025.61437.

Cardenas, J.D.C., Marín, J.G.A. and Toro, J.J.A. (2025) 'Numerical evaluation of the high solidity values effect on the performance of H-Darrieus turbine with NACA 0025 hydroprofil', *International journal of renewable energy development*, *14*(5), pp. 1072–1080. Available at: https://doi.org/10.61435/ijred.2025.61304.

Chen, Liu *et al.* (2023) 'Applied sciences aerodynamic enhancement of vertical-axis wind turbines using plain and serrated gurney flaps'. https://doi.org/10.3390/app132312643.

Dhanma, G.S. & Suryawan, A.A.A.S. dan A.G. (2018) 'Performance of ocean current power turbine model as alternative energy with NACA 0018 blade type', *Mechanical design engineering*, *7*(3), pp. 3–6.

Fadillah, A.Z. *et al.* (2024) 'Ocean thermal potential as new renewable energy in the waters of the east nusa tenggara islands using the ocean thermal energy conversion (OTEC)', *Jurnal EBT*, *5*(1), pp. 70–84. Available at: https://doi.org/10.14710/jebt.2024.22080.

Faisal, A.E. *et al.* (2026) 'Aerodynamic performance optimization of the archimedes spiral wind turbine : combined experimental and CFD analysis of step ratio and blade number effects', pp. 1–25. https://doi.org/10.1038/s41598-026-43165-9.

Fawaz, M.A. *et al.* (2026) 'Effect of blade parameters on radial turbine rotor aerodynamics', pp. 1–13. https://doi.org/10.1038/s41598-025-33442-4.

Fertani et al. (2025) 'Insights from the last decade in computational fluid dynamics (CFD) design and performance enhancement of darrieus wind turbines', *Jurnal*, 13, p. 370. Available at: https://doi.org/10.3390/pr13020370.

Firmansyah, et al. (2023) 'Design of ocean current blade turbine 500 kw using hydrodynamics simulation approach', *Journal of advanced research in fluid mechanics and thermal sciences*, *101*(1), pp. 174–185. Available at: https://doi.org/10.37934/arfmts.101.1.174185.

Ghadirian, F., Wan, H. & Chegini, S. (2025) 'A systematic analysis of a small-scale HAWT configuration and aerodynamic performance optimization through kriging, factorial, and rsm methods', *Jurnal*, *11*(4), pp. 887–903. Available at: https://doi.org/10.22055/jacm.2024.47896.4822.

Griego, A. et al. (2024) 'Development of a floating vertical axis wind turbine for the mediterranean sea development of a floating vertical axis wind turbine for the mediterranean sea'. Available at: https://doi.org/10.1088/1742-6596/2745/1/012008.

Gómez, M.A., Guevara-Muñoz, A. & Zuluaga, D.H. (2025) 'A numerical H Darrieus hydrokinetic turbine performance assessment with the application of openings in blade geometry', *International journal of renewable energy development*, *14*(1), pp. 1–9. Available at: https://doi.org/10.61435/ijred.2024.60514.

Haqiqi, J.F. (2018) 'Analysis of ocean current patterns in supporting the development of tidal power electricity in the toyopakeh strait, Nusa Penida, Bali', *Final project*. Surabaya.

Hatomi, F. (2011) 'CFD analysis of ocean current power plant turbine with a capacity of 1.2 Kw', *Thesis*.

Havis, M.I., Prasetyawan, I.B. & Widada, S. (2014) 'Location of turbine installation for ocean current power plant in Larantuka strait, east Flores', *Jurnal*, *3*(0), pp. 486–492. Available at: http://ejournal-s1.undip.ac.id/index.php/jose.

Jatmiko, D.T. *et al.* (2025) "Analysis of the potential of seawater energy resources in indonesia as an alternative source of electrical energy", 9, pp. 22262–22269.

Jiang, T. *et al.* (2026) 'Comparative study on aerodynamic performance of VAWTs with different airfoils under dimple-gurney flap synergistic control'. https://doi.org/10.3390/app16062882.

Khair, M. *et al.* (2021) "Study of the potential of renewable electricity generation using ocean currents in the jeneponto sea region," Journal of Makassar State University.

Lopulalan, R.M. (2016) 'Desain blade turbin pembangkit listrik tenaga arus laut di Banyuwangi berbasis CFD', *Jurnal teknik ITS*, *5*(2), pp. 424–430. Available at: https://doi.org/10.12962/j23373539.v5i2.19413.

Loutun, M.J.T. *et al.* (2021) '2D CFD simulation study on the performance of various naca airfoils', *CFD Letters*, *13*(4), pp. 38–50. Available at: https://doi.org/10.37934/cfdl.13.4.3850.

M. A. Chelabi, J.P. (2026) 'The effect of outlet blade angle at the mean root diameter on the mixed inflow turbine', *Jurnal*. Available at: https://doi.org/10.1038/s41598-026-52196-1.

Madi, M. *et al.* (2022) 'Experimental study of water flow deflector model to improve the performance of vertical type ocean current turbines at low current speeds', wave: *Scientific journal of maritime technology*, *15*(2), pp. 85–90. Available at: https://doi.org/10.29122/jurnalwave.v15i2.4954.

Madi, M. *et al.* (2025) 'Experimental investigation of convergent flow disturbances for performance enhancement of vertical-axis ocean current turbine at low current speed in indonesia', *Transactions on maritime science*, *14*(1), pp. 1–20. Available at: https://doi.org/10.7225/toms.v14.n01.012.

Marianus, s. et al. (2019) 'Application study of flywheels in micro hydro power plants (PLTMH)'.

Mark Jason, et al. (2021) 'Studi simulasi CFD 2D tentang kinerja berbagai airfoil NACA', *Jurnal ilmiah terapan*, *13*(4), pp. 38–50. Available at: https://doi.org/10.37934/cfdl.13.4.3850.

Michna, J. et al. (2024) 'A refined approach for Preset Blade Angle estimation and dynamic force hysteresis in H-type Darrieus wind turbines', *Energies*, *17*(24). Available at: https://doi.org/10.3390/en17246264.

Ministry of Energy and Mineral Resources. (2020). *Handbook of energy & economic statistics of Indonesia 2020*. https://www.esdm.go.id/id/publikasi/handbook-of-energy-economic-statistics-of-indonesia

Nayeri, C., Zheng, Z. and Chen, L. (2024) 'Aerodynamic performance and wake development of NACA 0018 airfoil with serrated gurney flaps', (May), pp. 1–14. Available at: https://doi.org/10.3389/fenrg.2024.1363402.

Prayoga, W.A. & Permatasari, R. (2019) 'Design and modeling of Darrieus turbine for ocean current power plant (PLTAL)', Machine, *10*(1). Available at: https://doi.org/10.25105/ms.v10i1.4127.

Presidential Regulation (2023) 'Presidential regulation of the republic of indonesia no. 11 of 2023 concerning additional concurrent government affairs in the energy and mineral resources sector in the new and renewable energy sub-sector', *Presidential regulation*.

Rahman, S., Baeda, A.Y. & Umar, H. (2016) "Potential of wave

energy as an alternative energy source in the outermost islands of the republic of indonesia," *Journal of engineering research (JRE)*, *20*(2), pp. 32–38.

Republic of Indonesia (2014) 'Government regulation of the republic of Indonesia no. 79 of 2014 concerning national energy policy', *Hukum online*, pp. 1–60.

Ramsyar, E. & Taufani, P.I. (2021) 'Prototype of ocean current power plant (PLTAL) using Darrieus type vertical axis turbine project', *Thesis*.

Rifai, T., Gunadi, G.G.R. & Ridwan, E. (2021) 'Design and construction of a savonius micro turbine wind power plant on the jatiasih toll road', *Applied mechanics journal, 2*(2), pp. 82–88. Available at: https://doi.org/10.32722/jmt.v2i2.4423.

Rogidio, M.C. *et al.* (2025) 'Influence of profile geometry on the self-starting capability of an H-Darrieus turbine', *International journal of renewable energy development*, *14*(4), pp. 694–702. Available at: https://doi.org/10.61435/ijred.2025.61124.

Sahid, S., Mulyono, M. & Arif Fauzi, D. (2024) 'Performance analysis of H-type Darrieus turbine radial projection blades based on NACA 0018', *Eksergi*, *20*(02), pp. 43–51. Available at: https://doi.org/10.32497/eksergi.v20i02.5806.

Şahin, İ. & Acir, A. (2015) 'Numerical and experimental investigations of lift and drag performances of NACA 0015 wind turbine airfoil', *International journal*, *3*(1), pp. 22–25. Available at: https://doi.org/10.7763/IJMMM.2015.V3.159.

Abu-Ela, M. S., ElRefaie, M. E., & Sayed, A. I. (2025). Enhancing vertical-axis wind turbine self-starting with distinctive blade airfoil designs. *Journal of engineering and applied science*, *72*(1), Article 95. https://doi.org/10.1186/s44147-025-0695-x.

Sudargana & Yuniarso, R.G.K. (2012) 'Analysis of Darrieus turbine design on hydrofoil NACA 0015 from cl and cd characteristics at variations of Preset Blade Angle using linear regression in matlab', *Rotasi*, *14*(1), pp. 21–28.

Syahputra, H. *et al.* (2014) 'Study of the potential of ocean currents as energy for power generation in the Larantuka strait, east Flores', journal, *3*(1), pp. 1–8. Available at: http://ejournal.undip.ac.id/index.php/buloma. https://doi.org/10.14710/buloma.v3i1.11212.

Uehiyori, K. & Shintake, T. (2025) 'Development of a horizontal-axis H-Darrieus turbine as a wave energy converter: semi-analytical study on coastal wave characteristics for conceptual design', *Energies*, *18*(6), pp. 1–17. Available at: https://doi.org/10.3390/en18061495.

Yunusa, H. A, Tokan, A. and Fachway, A.A. (2025) 'Design, simulation and optimization of NACA 0021 aerofoil blade using ansys fluent', *FUDMA Journal of Sciences (FJS*, *9*(12), pp. 42–51. Available at: https://doi.org/https://doi.org/10.33003/fjs-2025-0912-4295 8 FJS.

Zebedee, E., Jayaram, S. & Forbes, B. (2024) 'Enhancing energy capture efficiency of vertical axis wind turbines : a novel airfoil design with dynamic morphing potential', *Journal*. https://doi.org/10.2139/ssrn.5823483.

Zhang, B. *et al.* (2026) 'Mechanics aerodynamic optimization of variable-section j- shaped vertical axis wind turbine using feature- parameter microsegment dimension reduction method', 2060. Available at : https://doi.org/10.1080/19942060.2026.2665852.

Zhou, M. et al. (2025) 'Investigation of flow control on a vertical axis wind turbine using a bionic flap', *Journal*, (2019), pp. 823–837. Available at: https://doi.org/10.15632/jtam-pl/203691.